Multi-directional waves and time domain perturbed field visualization of the WaveSub device

Emilio Faraggiana, Ian Masters, John Chapman, Graham Foster and Gareth Stockman

Abstract— **Wave Energy Converters (WECs) are very often simulated in bi-dimensional waves but a more accurate simulation that represents a more realistic sea state should account for multi-directional waves. In a first approximation directional distribution can be expressed as a Gaussian spreading model. Here we show a simulation of the WaveSub device in multi-directional waves and a visualization of the perturbed field generated. Linear potential flow has been used for this purpose as compared to a CFD method used previously. Nemoh has been used for the hydrodynamic computation and for the calculation of the frequency domain field coefficients. The diffracted and radiated field calculation has been based also on the wave elevation and velocities result of a time domain simulation in WEC-Sim. Then the total perturbed field has been obtained as the sum of the incident, diffracted and radiated fields. Directional spreading has been modelled as a Gaussian spreading model. This result can give a reduced computational cost compared to CFD. The paper also presents a method for perturbed field visualization to show more confidence in the results obtained and this visualization could be used for future benchmarking purposes. Implementation of the multi-directional simulation has been completed in WEC-Sim and this modification to the software has been adopted in the official version. The authors recommend further cross-validation of the model should be carried out as further work.**

Keywords— **Directional distribution; wave energy; wave fields; wave potential theory.**

I. Introduction

Wave energy has been for many years a potential method of generation of renewable energy [1]. There are different problems that wave energy development needs to overcome for economic energy production. In fact, the wave energy resource is very difficult to predict accurately because of the temporal characteristic of the wave climate [2]. Variations are associated with modifications of the significant height, energy period and directional characteristics. Generally, WECs have a reduction of their performance when the wave directional spread is larger. Consequently, the estimation of the influence of the wave direction on a particular WEC should be considered carefully.

There are different concepts of wave energy extraction [3]. The WaveSub is a device under development by Marine Power Systems Ltd [4]. It is a point absorber device where the energy comes from the relative motion between a reactor and the float. An orbital motion is tracked by the float and the power is mainly captured in surge and heave in a similar way to the Bristol Cylinder [5]. Fig. 1 shows the working principle while more description is found in [6].

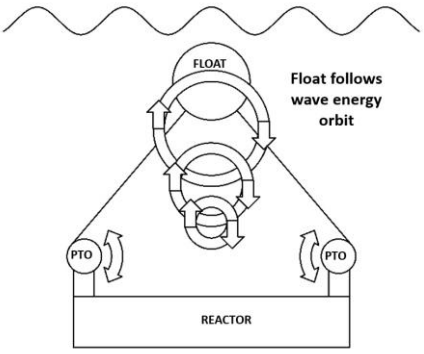

Fig. 1: Illustration of WaveSub device function in operational mode.

Power is captured by 4 float tethers, each one connected to a power take-off in each corner of the reactor. Fig. 2 shows the ¼ scale prototype WaveSub device. This paper aims to model the WaveSub under multi-directional waves. Diffracted, radiated and perturbed wave fields are

ID: 1232; TRACK: WHM. This research is supported by the Knowledge Economy Skills Scholarships (KESS 2). It is a pan-Wales higher level skills initiative led by Bangor University on behalf of the HE sector in Wales. It is part funded by the Welsh Government's European Social Fund (ESF) convergence programme for West Wales and the Valleys.

E. Faraggiana is with Marine Energy Research Group, College of Engineering, Swansea University, UK (e-mail: 951180@swansea.ac.uk).

I. Masters is with Marine Energy Research Group, College of Engineering, Swansea University, UK (e-mail: i.masters@swansea.ac.uk).

J. Chapman, G. Foster and G. Stockman are with Marine Power Systems Ltd, Ethos, King's Road, SA1 Swansea Waterfront, Swansea SA18AS, UK (e-mail: contact@marinepowersystems.co.uk).

 Copyright © European Tidal and Wave Energy Conference 2019

also calculated to show more confidence in the results obtained.

Fig. 2: Single float WaveSub on tow, showing the reaction barge in surface configuration with float docked in centre.

II. THEORY

Linear potential flow theory is the foundation of the numerical model [7]. Viscous forces are neglected. There are assumptions related to small motion of the device compared to its characteristic dimension and small wave amplitudes compared to the wavelength.
The Bernoulli equation is used in this theory but second order terms are neglected as shown in

$$\frac{\partial \phi}{\partial t} + \frac{1}{2}(\nabla \phi)^2 + \frac{p}{\rho} + gz = 0 \tag{1}$$

where ϕ is the fluid potential.
The radiation and the diffraction problem are then solved using the Boundary Element Method (BEM).

The dynamic system modelling, WEC-Sim [8] (Wave Energy Converter Simulator) is developed in MATLAB/SIMULINK. Multibody systems can be included in the simulation and hydrodynamic forces computed from Nemoh [9-10]. Power take-off and mooring systems can be also simulated in a realistic way.
The response of the device is obtained solving the equations of motion of the WEC in 6 degrees of freedom [11] as shown in

$$(m + A_\infty)\vec{X}'' = -\int_0^t K(t-\tau)\vec{X}'(\tau)d\tau + \vec{F}_{ext} + \vec{F}_{vis} + \vec{F}_{res} + \vec{F}_{PTO} + \vec{F}_{mo} \tag{2}$$

where m is the mass matrix, A_∞ is the added mass matrix, $\vec{X}$ is the displacement and rotational vector of the body, K is the matrix of impulse response function, $\vec{F}_{ext}$, $\vec{F}_{vis}$, $\vec{F}_{res}$, $\vec{F}_{PTO}$ and $\vec{F}_{mo}$ are the vector of wave-excitation force, quadratic viscous drag force, net buoyancy restoring force, PTO force and the mooring force.

A wave directional spreading is accounted in the time domain simulation regarding the calculation of the excitation force.

The directional distribution has been assumed to model with enough accuracy the temporal wave direction characteristic. More specifically, it is proposed that the frequency-directional spectrum ($S(f,\theta)$) is the product of the frequency spectrum ($S(f)$) and the directional distribution:
$S(f,\theta) = S(f)D(\theta)$
Where f is the wave frequency and θ is the angle relative to the mean wave direction.
The directional distribution ($D(\theta)$) is assumed to be independent of frequency. This result will give just an approximation. In-fact a more accurate directional distribution should be a function also of the frequency. Examples of directional spreading dependent also on the frequency are Mitsuyasu [12], Hasselmann [13], Donelan [14] and Donelan-Banner [15]. A general approach is shown in [16]. In particular, each climate location will have a different directional distribution.
The Gaussian directional distribution model has been chosen but a "cosine2s" form could be also used [17]. The Gaussian form is expressed as

$$D(\theta) = \frac{1}{\sigma\sqrt{2\pi}}\exp\left(-\left(\frac{\theta^2}{2\sigma}\right)\right) \tag{3}$$

where σ is the standard deviation and θ is the incident wave direction.
The directional distribution fulfils the requirement

$$\int D(\theta,\omega)d\theta = 1 \tag{4}$$

The sea surface elevation dependent also on the wave directions can be expressed as

$$\eta(x,y,t) = \sum_{n=1}^{N_f}\sum_{m=1}^{N_d} A_{I,ij}\cos\big(2\pi f_n t - k_n \cdot (x\cdot cos(\theta_m) + y\cdot sin(\theta_m)) + \Phi_{I,nm}\big) \tag{5}$$

where $A_{I,nm}$, f_n, k_n, $\Phi_{I,nm}$ are respectively the amplitude, frequency, wave number and phase for each incident directional wave evaluated for a specific point of the wave field (x,y). N_d and N_f are the number of wave directions and frequencies.

The directional spread and the excitation force for multi-directional waves have been the main updates applied to the WEC-Sim code.
Sea surface elevation can be then expressed as a function of the wave frequency spectrum thanks to the relation

between the wave amplitudes and the wave spectrum. The relation is expressed for a discretized frequency step (Δf) as [18]

$$A_{I,\mathrm{nm}} = \sqrt{2S(f_n)D_m\Delta f} \tag{6}$$

Consideration of the wave directional spread also requires an update of the calculation of the excitation force. The extended formulation of the excitation force in the time domain is expressed as

$$\begin{aligned}\vec{F}_{ex}(t) &= \sum_{\mathrm{n}=1}^{N_f}\sum_{\mathrm{m}=1}^{N_d}\sqrt{2S(f_n)D_m df}\\ &\cdot Re\left(\vec{F}_{ex\_n}\right.\\ &\cdot \exp\left(i2\pi f_n t + \Phi_{I,\mathrm{nm}}\right)\Big)\\ &= \sum_{i=1}^{Nf}\sum_{j=1}^{N_d}\sqrt{2S(f_n)D_m df}\\ &\cdot \Big(Re\left(\vec{F}_{ex\_n}\right)\\ &\cdot \cos\left(2\pi f_n t + \Phi_{I,nm}\right)\\ &- Im\left(\vec{F}_{ex\_n}\right)\\ &\cdot \sin\left(2\pi f_n t + \Phi_{I,nm}\right)\Big)\end{aligned} \tag{7}$$

where the excitation force is a complex number described by an amplitude and phase.

The perturbed wave field is helpful to create more confidence and observe the interaction between the WEC and the wave field. Results have been elaborated from material obtained from Cruz Atcheson Consulting Engineering [19]. Wave fields are summarized in the incident, diffracted, radiated and perturbed fields. The visualization involved 2 main software: Nemoh and WEC-Sim.

Nemoh and WEC-Sim have an opposite notation of the incoming incident wave direction and the following formulae have been adapted to the Nemoh notation. Nemoh needs to be simulated using the free surface elevation option. In particular, the size of the domain and the number of points in x and y dimensions are defined. This option increases significantly the computational time of Nemoh. A free surface elevation file is created for each frequency, wave direction and degree of freedom considered. Wave direction is related with the diffracted field while the number of degrees of freedom with the radiated field. The number of files generated follows

$$\begin{aligned}N_{total} &= N_{Diffracted} + N_{Radiated}\\ &= N_f \cdot (N_d + N_{DoF})\end{aligned} \tag{8}$$

The incident wave elevation and the bodies velocities from WEC-Sim have been converted into the frequency domain using the Fourier transform. The same hydrodynamic Nemoh frequencies have been used in this conversion to match the free surface generation files generated by Nemoh. The hydrodynamic frequency step and the WEC-Sim simulation time step have been related using the reciprocity relations to approximate in the best way the bodies velocities and the incident wave elevation. This relation can be expressed as [20]

$$\Delta f \cdot \Delta t = \frac{1}{L} \tag{9}$$

Where Δf is the hydrodynamic frequency step, Δt is the WEC-Sim simulation time step and L is the length of the signal.

The Fourier transform has been used to find the amplitude and phases of the incident wave and of the bodies velocities as shown in

$$F(\omega) = \frac{2}{T_{sim}}\int\sum_{\mathrm{n}=1}^{N_f}(f(t)\cdot e^{i2\pi f_n t})dt \tag{10}$$

where T_{sim} is the duration of the signal and $f(t)$ is the value of the signal at the time t.

After that the time domain wave fields are determined considering the real part for each point P(x_P, y_P) of the wave field as shown in

$$\eta_{IP}(t) = Re\left(\sum_{\mathrm{n}=1}^{N_f}\sum_{\mathrm{m}=1}^{N_d}A_{I,ij}e^{i\left(K_{nmP}-2\pi f_n t+\Phi_{I,\mathrm{nm}}\right)}\right) \tag{11}$$

$$K_{nmP} = k_{nP}\cdot(x_P\cdot\cos(\theta_m) + y_P\cdot\sin(\theta_m)) \tag{12}$$

$$\begin{aligned}&\eta_{DP}(t)\\ &= Re\left(\sum_{\mathrm{n}=1}^{N_f}\sum_{\mathrm{m}=1}^{N_d}A_{I,\mathrm{nm}}A_{DPnm}e^{i\left(-2\pi nt+\Phi_{I,\mathrm{nm}}+\Phi_{DPnm}\right)}\right)\end{aligned} \tag{13}$$

$$\begin{aligned}&\eta_{RP}(t)\\ &= Re\left(\sum_{\mathrm{n}=1}^{N_{DoF}}\sum_{\mathrm{m}=1}^{N_f}V_{nm}A_{RPnm}e^{i\left(-2\pi f_n t+\Phi_{\mathrm{Vnm}}+\Phi_{RPnm}\right)}\right)\end{aligned} \tag{14}$$

where A_{DPnm} and Φ_{DPnm} are the amplitude and phase of the diffracted field, A_{RPnm} and Φ_{RPnm} are the amplitude and phase of the radiated field, V_{nm} and Φ_{Vnm} are the amplitude and phase of the bodies velocities. η_{IP}, η_{DP}, η_{RP}

are respectively the incident, diffracted and radiated wave fields.

A summary of the amplitude and phase obtained from Nemoh and WEC-Sim is shown in the following Table 1:

Table 1: Summary of the Wave field parameters

	Nemoh	WEC-Sim
Incident Field	θ, f	$A_I, k, \theta, f, \Phi_I$
Diffracted Field	A_D, Φ_D	A_I, ω_i, Φ_I
Radiated Field	A_R, Φ_R	$V, \Phi_V,$

Finally, the total perturbed wave field can be calculated:

$$\eta_{PP}(t) = \eta_{IP}(t) + \eta_{DP}(t) + \eta_{RP}(t) \tag{15}$$

Wave fields in the frequency domain are obtained using (11-15) but without accounting the time term $-2\pi f_i t$ of the exponential term. The frequency wave field considers the complex results and not the real one because it gives information both of the amplitude and of the phase. The significant height can be used to describe the frequency wave fields and, following the method of [6], can be expressed for each point P(x_P, y_P) of the wave field:

$$H_{sP} = 4\sqrt{\sum_{n=1}^{N_f} \frac{abs(\eta_{Pn}(f))^2}{2}} \tag{16}$$

The significant height for multi-directional waves can be obtained from the surface elevation in the frequency domain through the summation for all the wave directions.

$$\eta_P(f) = \sum_{m=1}^{N_d} \eta_P(f, \theta) \tag{21}$$

III. METHODOLOGY

The core of the numerical simulation is the combination of two open-source software: Nemoh and WEC-Sim. The first computes hydrodynamic coefficients and the second the time domain simulation of the device and shown in Fig. 3. WEC-Sim source code has been modified accounting the influence of the wave directional distribution on the excitation force. This modification has been applied to the WEC-Sim linear model but could be theoretically extended to the weak non-linear model considering the non-linear Froude-Krylov force based on the dynamic pressure over each panel of the wetted body surface.

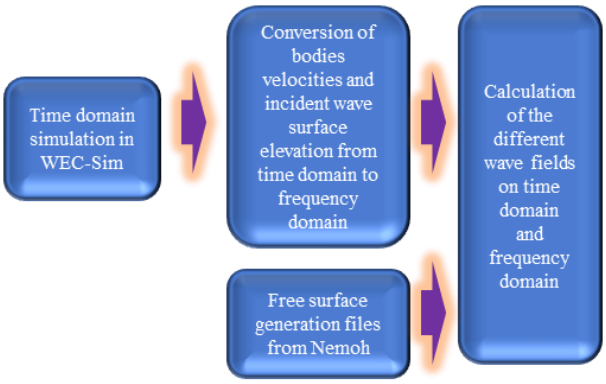

Fig. 3: The overview of the calculation of the wave fields

The wave directional distribution has been based on the average wave directional standard deviation (28.95 degrees) of the Berth A wave buoy in the Belmullet site [21]. Wave directions between the main direction and 2 times the wave direction spread can be simulated to give a probability of 95.45% of the real incoming directional wave (See Fig. 4). The normal distribution has been discretized in 7 wave directions with a related probability.

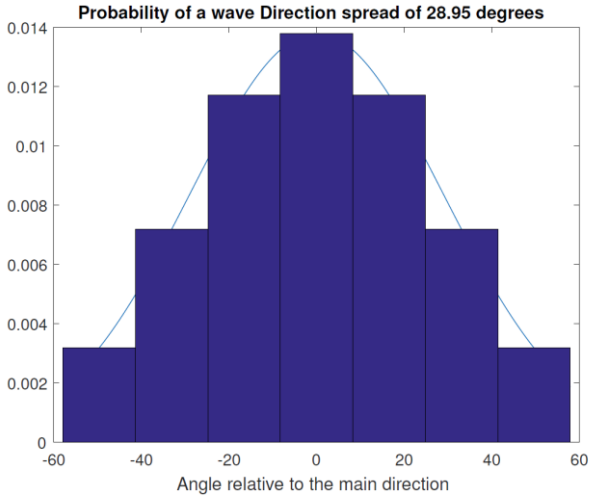

Fig. 4: The discretization of the directional distribution

IV. COMPUTATIONAL MODEL SET-UP

An irregular wave described by a Pierson-Moskowitz Spectrum with a significant height of 3m and a peak period of 10s is considered.

Pierson-Moskowitz is expressed as a function of the peak period and the significant height following [8] and [22]. More details about the equations used for the wave Spectrum are given in the source code of WEC-Sim [8]. The simulation of this wave Spectrum through these formulae is obtained in WEC-Sim using a specific simulation option of the "Waveclass" [8]. Two different main wave configurations have been used: a single wave direction and a multi-wave direction.

A reasonable number of frequencies (952) have been used for the hydrodynamic simulation between 0.02 and 5 rad/s. The number of field points used is 50 points in x and y while the field area covers 100m in each dimension. So each point covers an area of 4m². If local effects are targeted, this could require an increase in the resolution.

Equation (9) shows a relation between the frequency step and the time step. The simulation time for WEC-Sim is determined from the frequency step of the Nemoh frequencies. In particular a simulation time of 1202s has shown a good approximation of the time domain incident wave field and of the bodies velocities through the Fourier transform.

A single float WaveSub configuration have been used for the simulations. The inertia properties and the hydrodynamic coefficients are based on the simplified version of the WaveSub. (a cuboid shape for the reactor and a cylinder and 2 hemispheres for the float). Size and measurements come from the full scale representation of the tank testing conducted at the University of Plymouth Ocean basin in 2016 [23]. The reactor is simplified as a cuboid shape with length, width and height respectively of 51.55, 50 and 10.5m. The float is described by a central cylinder with a length of 4.75m and 2 hemispheres in the sides with a diameter of 12m. The float depth is of 10.55m while the reactor depth is arbitrary chosen and in this configuration a value of 33m has been used as an example.

A mesh independence study has been undertaken to make sure that the hydrodynamic results were not dependent on the mesh resolution. The main direction (0 degrees relative to the x axis) has been chosen in this analysis.

The mesh of the bodies has been created in Salome-Meca [24]. Panels can be created mainly triangular or quadrangular.

Three types of mesh have been considered: a coarse (201 panels for the float and 200 for the reactor), a moderate (547 panels for the float and 877 for the reactor) and a fine mesh (868 panels for the float and 1501 for the reactor.

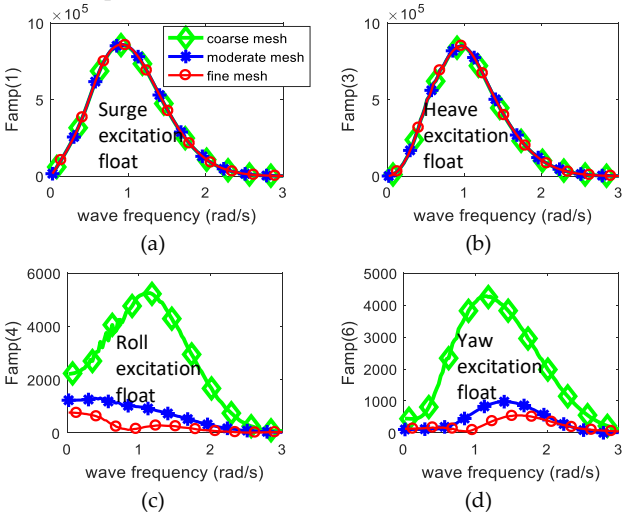

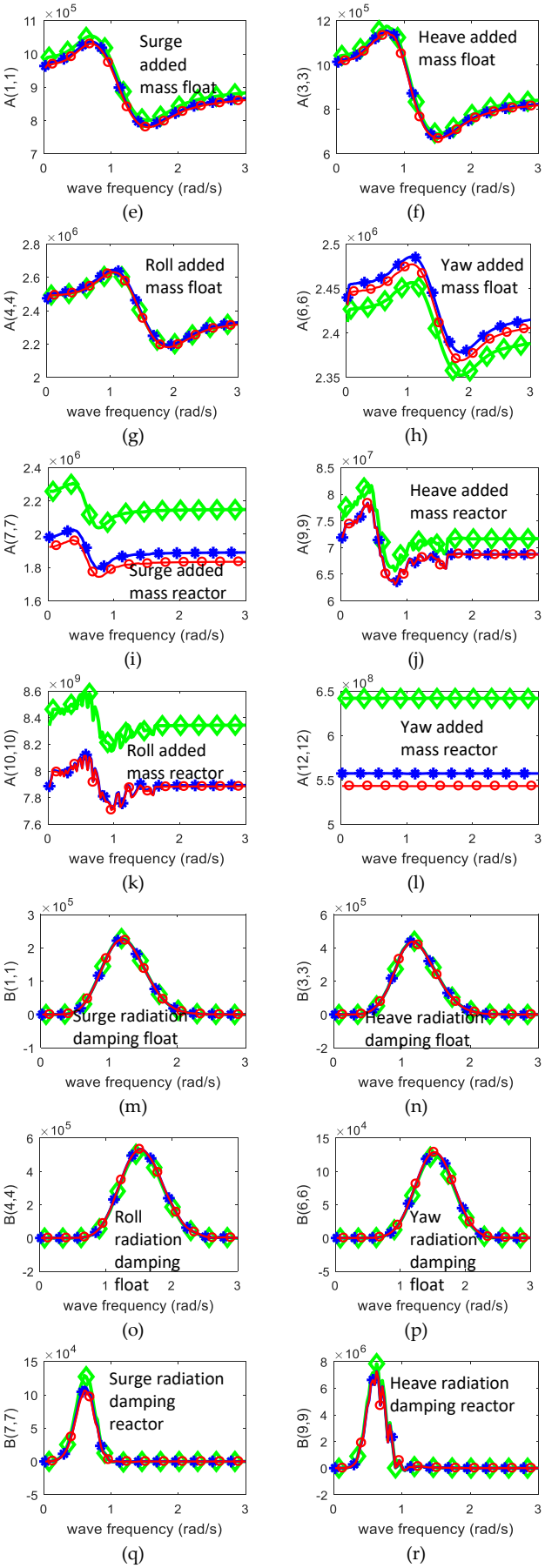

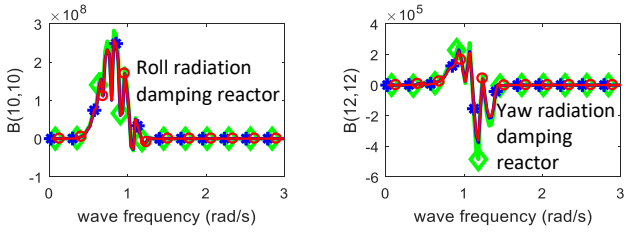

Fig. 5: Surge, heave, roll and yaw excitation coefficients of float (a,b,c,d), surge, heave excitation coefficients of reactor (e,f), surge, heave, roll and yaw added mass coefficients of float for surge, heave, roll and yaw motion of the float (g,h,i,j), surge, heave, roll and yaw added mass coefficients of reactor for surge, heave, roll and yaw motion of the reactor (k,l,m,n), surge, heave, roll and yaw radiation damping coefficients of float for surge, heave, roll and yaw motion of the float (o,p,q,r), surge, heave, roll and yaw radiation damping coefficients of reactor for surge, heave, roll and yaw motion of the reactor (s,t,u,v).

A good mesh convergence can be observed from Fig. 5. Main motion for a main single wave direction is expected to be in surge, heave and pitch due to the symmetry of the device relative to the wave direction. It is expected that the excitation coefficients in the others degrees of freedom are negligible. In fact, it is found that excitation force in roll and yaw is around 100 times smaller than in surge and heave (See Fig. 5a-5b-5c-5d). It is converging to zero with an increasingly fine mesh.

By contrast, radiation coefficients are significant in all the degrees of freedom but the force is only present in some directions because it is dependent on the velocity and acceleration of the device in each degree of freedom (radiation damping and added mass force respectively). Added mass force and radiation damping force will be more significant in the degrees of freedom where the excitation force is determining a more significant velocity and acceleration of the body.

Added mass and radiation damping of the reactor show the problem of Nemoh related to thin elements (See Fig. 5j-5k-5r-5s-5t). The behaviour of these coefficients are irregular for some frequencies and it is a known limitation of Nemoh. Nemoh is based on a source distribution and the computation of thin elements could have created this irregularity. In-fact the shape of the reactor has the height 5 times smaller than the other 2 dimensions.

Finally, the fine mesh has been used because of the higher accuracy.

The PTO and the mooring system are characterized by 5 and 4 lines. Each line of the PTO, that connects each float and the reactor, is described by a linear spring and damper with a constant stiffness and damping. Each line of the mooring, that connects each corner of the reactor and the seabed, is instead described by only a constant stiffness spring.

The drag force on each float was difficult to determine accurately [25]. A previous research of Marine Power Systems has been used for an estimation of the drag coefficient of 1.5 [26]. A comparison with the drag coefficient of spheres and cylinders have been used for the estimation of the drag coefficient of the float [27].

A drag force has been considered only for the float but not for the reactor because it becomes more significant relative to the inertia force when the characteristic dimension is less than 1/5 of the shortest wavelength [28]. Drag coefficient depends on different a-dimensional numbers such as the Keulegan-Carpenter number, Reynolds number and the surface roughness. However the data available are limited and due to the shape of the float (a mix between cylinders and hemispheres) an accurate result cannot be achieved. A recent paper investigates this effect further [25].

The relation between drag coefficient and drag force used in the model is the following:

$$\vec{D} = \frac{1}{2} C_d \rho A \vec{v} |\vec{v}| \tag{26}$$

Where A is the characteristic area of the body, v is the body velocity, C_d is the drag coefficient, D is the drag force and ρ is the density.

V. Results

Results are presented in terms of a single wave direction and a multi-wave direction. A multi-wave direction simulation is more computationally demanding because it requires the hydrodynamic simulation for all the wave directions used for the approximation of the directional distribution. Then the time domain simulation is also longer because the excitation force is computed considering all the wave directions.

Fig. 6 shows the significant motions for the float and the reactor in all the degrees of freedom. Main motion for the 1 incident wave direction case is in surge, heave and pitch. This conclusion was already observed in the mesh convergence due to the largest excitation coefficients in these degrees of freedom.

Overall, the motion in these degrees modes decreases for the float considering the directional wave distribution while sway, roll and yaw become more important. The reactor shows also a similar motion behaviour. However, the wave directional distribution case shows a slight increase in the heave motion.

A. Single wave direction

Frequency and time domain results are presented for the different wave fields (See Fig. 7 and Fig. 8). The significant height of the incident field is not shown because this is constant and equal to 2.91 m. A better accuracy of the significant height equal to 3 m can be reached with a longer simulation time that however, corresponds to a larger number of hydrodynamic frequencies considered in the simulation. The diffracted field generates an increase of the significant height behind the device while the radiated field shows an increase in the front and in the back of the

device. The relative difference between the total significant height and the incident wave height is shown in Fig. 7 to observe more clearly the influence of the radiation and diffraction wave fields on the total significant height and the positive increases. The total significant height has mainly an increase in the front while behind the device there is an increase further from the float. This different behaviour of the total wave field compared to the diffracted and radiated wave fields is due to the total wave field considering the phases of each wave field. So, the perturbed wave field shows generally a smaller significant height behind the device compared to the incident wave height. A larger value of the significant height follows more or less a parabolic curve centered on the float.

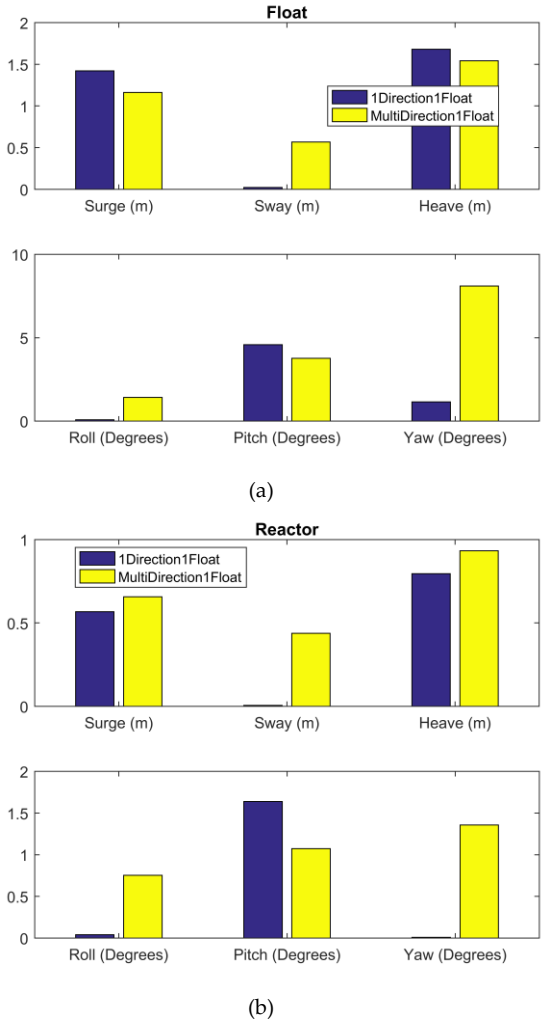

Fig. 6: Significant motions of the float (a) and of the reactor (b) in all the degrees of freedom. A comparison between the 1 direction and the directional distribution is shown.

Fig. 8 shows a screenshot of the time domain of the incident and perturbed wave fields. In particular, it is possible to observe an expected increase of the perturbed wave field behind the float. The time domain visualization is valuable in a commercial context, because it shows in a very direct way if the results are reasonable or if they are the results of numerical errors. It is a first step to understand the numerical model that is to be used in parallel to a more formal validation process.

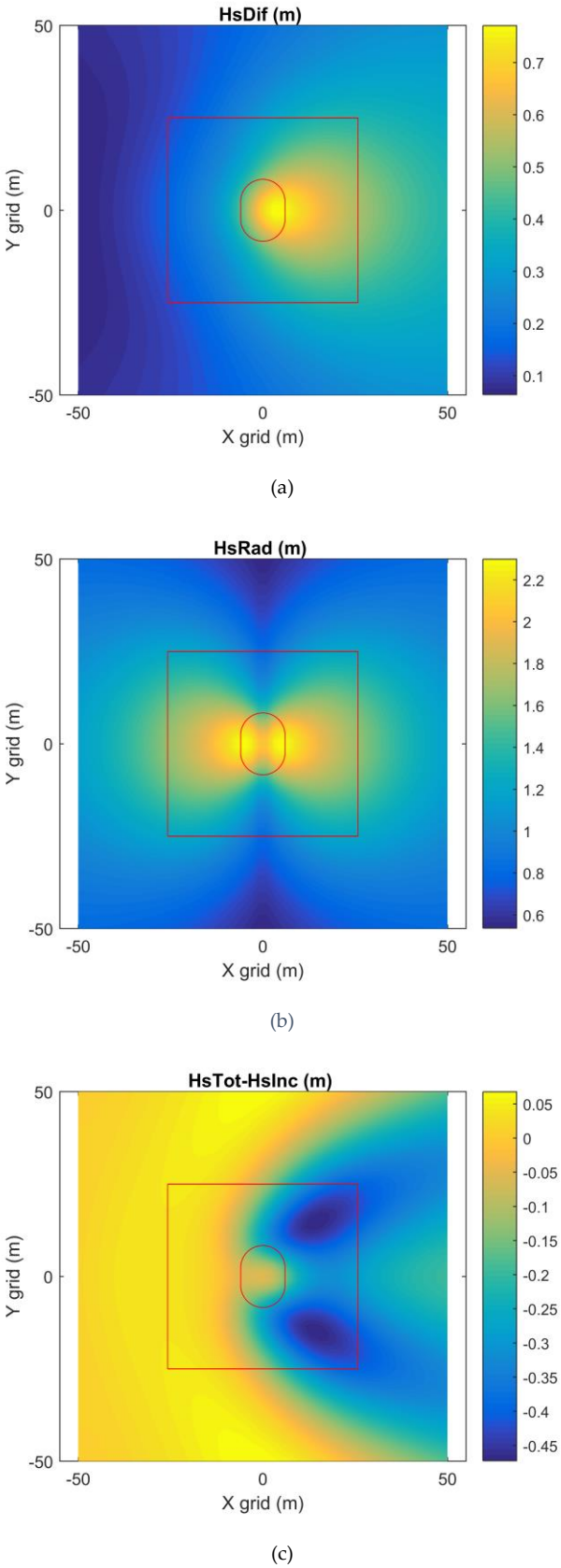

Fig. 7: Significant heights created by the diffraction (a), radiation (b) and perturbed (c) fields for a single wave direction case.

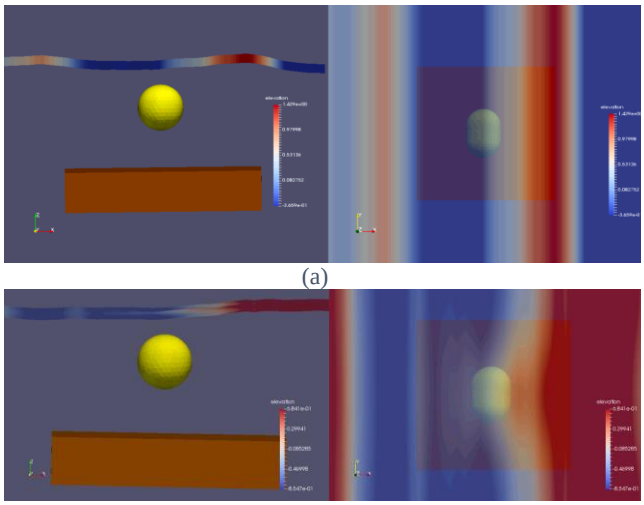

(a)

(b)

Fig. 8: Screenshot of the time domain simulation created in Paraview [29] showing the incident (a) and the perturbed (b) fields for a single wave direction case. Only float and reactor are shown while PTO lines and mooring lines are omitted.

B. Multi-directional waves

The significant height of the incident wave field shows a different value in each point of the wave field due to the dependence on the wave direction (See Fig. 9). The random phase related to the wave direction and wave frequency and the different location of the wave field are determining this variation (Refer to (5)). However, it is expected that there will be convergence of the incident significant height for all the grid points to the incident wave height (3m) for a very long simulation time. The significant wave height of the diffracted field shows a similar behaviour of the single wave direction but it is decreased. The radiated significant wave height reaches larger values not anymore along the main wave direction but along a certain relative angle to the main wave direction due to the different motion of the device (also in sway). The total significant height shows a narrower shading behind the device compared to a single wave direction.

Fig. 10 shows a snapshot of the time domain simulation. In particular it is shown when the incident field has a wave direction different from mean. It is possible to observe the wave field with different local peaks dependent on both the coordinates of the grid. The float is observed during a yaw motion due to a wave directional component coming from south-west.

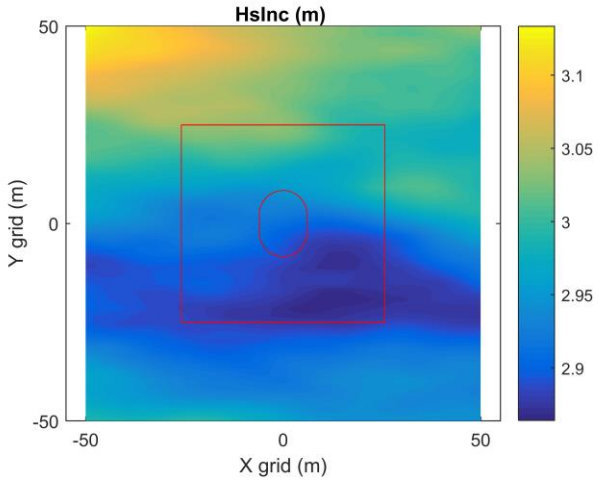

(a)

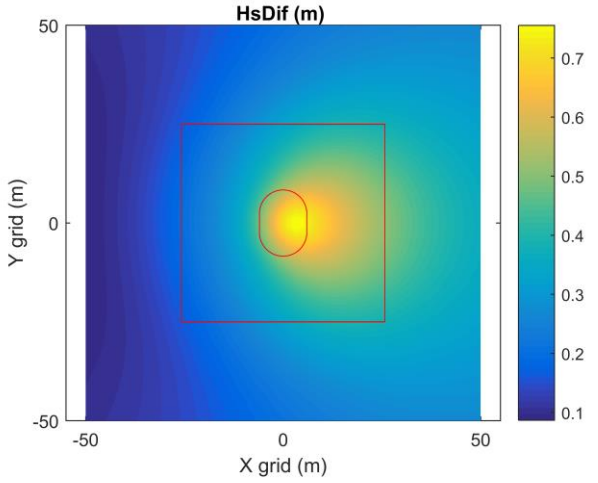

(b)

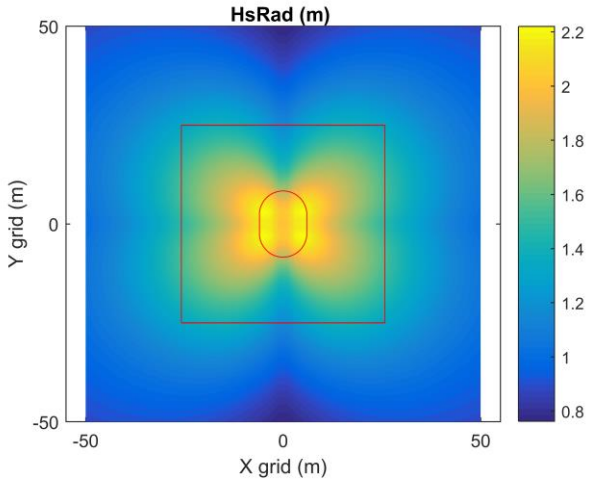

(c)

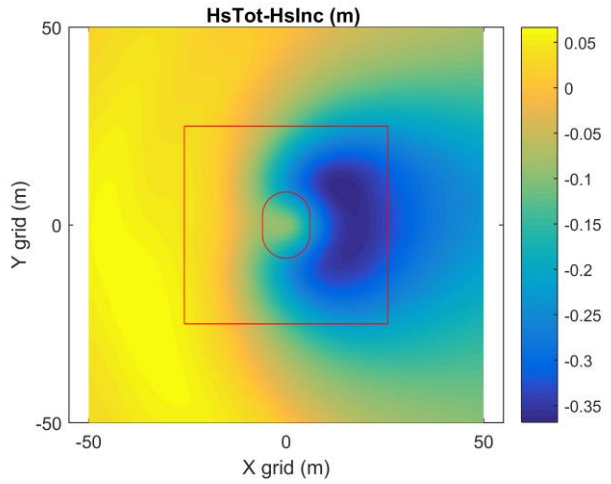

(d)

Fig. 9: Significant heights created by the incident (a), diffraction (b), radiation (c) and perturbed (d) fields for a multi-wave direction case.

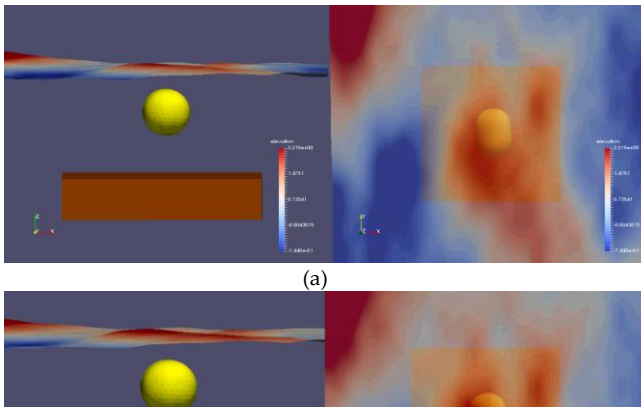

(a)

(b)

Fig. 10: Screenshot of the time domain simulation created in Paraview [29] showing the incident (a) and the perturbed (b) fields for a multi-wave direction case. Only float and reactor are shown while PTO lines and mooring lines are omitted.

VI. Conclusion

Multi-directional waves and wave fields have been modelled and analysed. The WaveSub device has been considered as a reference for this purpose. The results show the influence of the device on the significant height of the wave fields. These are the incident, the diffracted, the radiated and the perturbed wave fields. Then a time domain visualization is also given. The time domain visualization gives more confidence of the results obtained.

A comparison between a single wave direction and multi-directional waves is described. The WaveSub device moves mainly in surge, heave and pitch for a single wave direction due to the symmetry of the device relative to the wave direction. As expected the device starts moving also in the others degrees of freedom when subjected to multi-directional waves.

Finally, the total significant wave height is mainly reduced behind the device while an increase of it follows a parabolic shape for a single wave direction. Diffracted significant wave height has an increase behind the device while the radiated significant wave height has an increase in the front and behind the WaveSub device.

Further work will include a comparison and validation with results coming from tank testing. Additionally, the directional distribution could be still investigated for a more realistic relationship with the frequency.

Acknowledgement

This research is supported by the Knowledge Economy Skills Scholarships (KESS 2). It is a pan-Wales higher level skills initiative led by Bangor University on behalf of the HE sector in Wales. It is part funded by the Welsh Government's European Social Fund (ESF) convergence programme for West Wales and the Valleys.

References

[1] João Cruz, "Ocean wave energy: current status and future perspectives", Springer Science & Business Media, 2007

[2] A. Pecher and J. P. Kofoed, "Handbook of Ocean Wave Energy", SpringerOpen, 2017

[3] António F. de O. Falcão, "Wave energy utilization: A review of the technologies", Renewable and Sustainable Energy Reviews, Volume 14, Issue 3, 2010

[4] http://marinepowersystems.co.uk/ , accessed: 2017-09-01.

[5] R. Clare, D. V. Evans, T. L. Shaw, "Harnessing sea wave energy by a submerged cylinder device", Proceedings of the Institution of Civil Engineers, 1982

[6] Chapman, J., Perez Torres, D. , Baldini, A., Le Dreff, J.B., Masters, I., Foster, G., Stockman, G., Greaves, D., Iglesias, G., "Validation of Storm Load Limitation of a Novel Wave Energy Convertor using Scale Model Testing", Proceedings of the 11th European Wave and Tidal Energy Conference 6-11th Sept 2015, Nantes, France.

[7] A. F. Falcão, "Modelling of wave energy conversion," Instituto Superior Técnico, Universidade Técnica de Lisboa, 2013.

[8] https://github.com/WEC-Sim/WEC-Sim , accessed: 2017-09-01.

[9] https://lheea.ec-nantes.fr/logiciels-et-brevets/nemoh-presentation-192863.kjsp ,accessed: 2017-09-01.

[10] Babarit, A. & G. Delhommeau (2015). Theoretical and numerical aspects of the open source bem solver nemoh. In 11th European Wave and Tidal Energy Conference (EWTEC2015).

[11] Babarit, Aurélien, et al. "Numerical benchmarking study of a selection of wave energy converters." Renewable energy 41 (2012): 44-63. Mitsuyasu, H., and Coauthors, 1975: Observations of the directional spectrum of ocean waves using a cloverleaf buoy. J. Phys. Oceanogr., 5, 750–760.

[12] Mitsuyasu, H., and Coauthors, 1975: Observations of the directional spectrum of ocean waves using a cloverleaf buoy. J. Phys. Oceanogr., 5, 750–760.

[13] Hasselmann, K., and Coauthors, 1973: Measurements of wind-wave growth and swell decay during the Joint North Sea Wave Project (JONSWAP). Dtsch. Hydrogr. Z, 8 (Suppl. A), 5–95.

[14] Donelan, M. A., J. Hamilton, and W. H. Hui, 1985: Directional spectra of wind-generated waves. Philos. Trans. Roy. Soc. London., A315, 509–562.

[15] Banner, M. L., 1990: Equilibrium spectra of wind waves. J. Phys. Oceanogr., 20, 966–984.

[16] Kevin C. Ewans, Observations of the Directional Spectrum of Fetch-Limited Waves, Shell International Exploration and Production B.V, The Hague, the Netherlands, 1997

[17] T. Adcock and P. Taylor, "Estimating ocean wave directional spreading from an eulerian surface elevation time history," in Proceedings of the Royal Society of London A: Mathematical, Physical and Engineering Sciences, vol. 465, no. 2111. The Royal Society, 2009, pp. 3361–3381.

[18] A. F. Falcão, "Modelling of wave energy conversion," Instituto Superior Técnico, Universidade Técnica de Lisboa, 2013.

[19] Y. Debruyne, "User and theory manual: Free-surface visualisation tool," Cruz Atcheson Consulting Engineering, 2017.

[20] OSGOOD, B. EE 261-The Fourier transform and its applications. Electrical Engineering Department: Stanford University, 2007.

[21] http://www.oceanenergyireland.ie/TestFacility/AMETS, accessed: 2018-04-04.

[22] TUCKER, Malcolm John; PITT, Edward G. Waves in ocean engineering. 2001.

[23] C. Whitlam, "The multi float wavesub wave energy convertor (wec)," in IUK Project 132402, 2017.

[24] Code Aster (2018). Salome-Meca. Available at: https://www.code-aster.org/spip.php?article303 (May 2018).

[25] E. Faraggiana, C. Whitlam, J. Chapman, A. Hillis, J. Roesner, M. Hann, D. Greaves, Y-H. Yu, K. Ruehl, I. Masters, G Foster, G, Stockman, "Computational modelling and experimental tank testing of the multi float WaveSub under regular wave forcing", "under review".

[26] Marine Power Systems Ltd, "Research of drag coefficients for the float of the wavesub", Swansea, Tech. Rep.

[27] T. Sarpkaya, Wave forces on offshore structures. Cambridge university press, 2010.

[28] A. Ansys, "Theory manual. release 15.0," 2013.

[29] https://www.paraview.org/, accessed: 2019-02-07.